Antarctic Science (2025), **00**, 1–13
doi: 10.1017/S0954102025100205

CAMBRIDGE UNIVERSITY PRESS

Biological Sciences

Assessing the relationship between viruses and protists and their role in dimethylsulphoniopropionate release in Antarctic surface microlayers

Dolors Vaqué, Elisa Berdalet, Ana Sotomayor-Garcia, Marta Estrada, Miguel Cabrera-Brufau, Marta Masdeu-Navarro, Arianna Rocchi, Xabier López-Alforja, Magda Vila, Cèlia Marrasé, Rafel Simó, Manuel Dall'osto and Maria Montserrat Sala

Institut de Ciències del Mar (CSIC), Barcelona, Catalunya, Spain

Abstract

Marine microorganisms play a crucial role in biogeochemical cycles, especially in the surface microlayer (SML), which differs from adjacent subsurface waters (SSW). In this study, we sampled the SML and SSW at 20 sites along the western Antarctic Peninsula during the summers of 2015 and 2019, examining microbial, viral and environmental differences. We focused on phototrophic protists, specifically *Phaeocystis*-like species, known for their high dimethylsulphoniopropionate (DMSP) contents, which can be released through viral lysis. DMSP is a precursor to dimethylsulphide (DMS), a gas influencing Earth's climate. We hypothesized a significant relationship between *Phaeocystis*-like abundance and DMSP concentration, with strong interactions with their specific viruses (V4) in the SML. Most biotic variables showed higher mean values in the SML, although these differences often were not statistically significant. DMSP concentrations correlated with *Phaeocystis*-like species abundance in both layers ($R^2 = 0.482$, $P \leq 0.01$; $R^2 = 0.532$, $P \leq 0.01$, respectively), whereas V4 abundance significantly correlated with *Phaeocystis*-like species only in the SML ($R^2 = 0.572$, $P \leq 0.01$). These results suggest stronger interactions between viruses and DMSP-rich hosts in the SML, potentially increasing DMS emissions to the atmosphere and impacting climate regulation.

Keywords: DMSP; *Phaeocystis*-like species; phototrophic nanoflagellates; virus V4; western Antarctic Peninsula

(Received 24 October 2024; revised 4 May 2025; accepted 17 May 2025)

Introduction

The sea surface microlayer (SML), the < 1000 µm-thick water layer at the boundary between the ocean and the atmosphere, is an extensive habitat covering 70% of the Earth's surface (Liss & Duce 1997). The SML has distinct physicochemical and biological properties compared to the underlying waters (Cunliffe *et al.* 2009). It is considered to be a fundamental environment for biogeochemical cycling and has a potential influence on air-sea exchange processes such as gas transfer (via volatilization) and sea spray aerosol formation by bubble bursting associated with breaking waves, mechanical tearing and spilling of wave crests (Cunliffe *et al.* 2013, Engel *et al.* 2017, Sellegri *et al.* 2021).

In the SML, inorganic nutrients and organic components (transparent exopolymers, dimethylsulphoniopropionate (DMSP), lipids, carbohydrates, amines, etc.) accumulate together with microorganisms such as viruses, prokaryotes and protists (phototrophic and heterotrophic; Cunliffe *et al.* 2013). This accumulation favours the development of SML-associated microbial communities (Hardy 1982, Kuznetsova & Lee 2001, Rahlff 2019, Martínez-Varela et al. 2020), whose composition can be more variable than that in the subsurface waters (SSW) due to exposure to greater solar ultraviolet (UV) radiation, changes in atmospheric temperature and wind speed, salinity gradients, toxic organic substances and heavy metals (Hardy 1982, Tovar-Sanchez et al. 2019).

Microorganisms and viruses play a pivotal role in ocean biogeochemistry, particularly within the SML, where their interactions are likely to be more pronounced due to the reduced space (Vaqué et al. 2021). This feature has been extensively investigated in temperate systems (Nakajima *et al.* 2013, Rahlff *et al.* 2019, Zäncker *et al.* 2021), yet they remain poorly studied in polar systems. Nevertheless, the available information in Antarctic and Arctic systems (e.g. Tovar et al. 2019, Vaqué et al. 2021) suggests that the SML harbours high microbial production and high viral activity. The interactions among microorganisms and the subsequent biogeochemical processes can be sources of metabolites that act as direct or indirect precursors of aerosols (Matrai *et al.* 2008, Dall'Osto *et al.* 2017). Thus, the interaction between viruses

Corresponding author: Dolors Vaqué; Email: dolors@icm.csic.es

Cite this article: Vaqué, D., Berdalet, E., Sotomayor-Garcia, A., Estrada, M., Cabrera-Brufau, M., Masdeu-Navarro, M., Rocchi, A., López-Alforja, X., Vila, M., Marrasé, C., Simó, R., Dall'osto, M., & Sala, M. M. 2025. Assessing the relationship between viruses and protists and their role in dimethylsulphoniopropionate release in Antarctic surface microlayers. *Antarctic Science*, 1–13. https://doi.org/10.1017/S0954102025100205

and their specific photosynthetic eukaryotic hosts may be a contributing factor in the release of aerosol precursors from cells, their enrichment in the SML and their subsequent transformation and emission to the atmosphere (Hill *et al.* 1998).

During the summer in the Southern Ocean, significant phytoplankton blooms occur (Tréguer et al. 1992), generally followed by the proliferation of prokaryotes, heterotrophic protists and viruses (Gowing *et al.* 2004, Sotomayor-Garcia *et al.* 2020). The SML can contain great abundances and high levels of activity and diversity of these microorganisms (Obernosterer *et al.* 2008, Vaqué et al. 2021). The grazing of protists and/or zooplankton (through sloppy feeding; i.e. incomplete ingestion and digestion of prey) and viral lysis on prokaryotes and phytoplankton (as observed by Engel *et al.* 2017 and references therein) promote the leaching of organic matter and secondary metabolites. A notable secondary metabolite is DMSP, an algal osmolyte that is produced in high intracellular concentrations by numerous phytoplankton taxa, including haptophytes, cryptophytes and small dinoflagellates (Simó 2001, Steiner *et al.* 2019). DMSP is released from cells primarily through senescence or exudation during the late phases of phytoplankton blooms (Matrai & Keller 1994, Laroche *et al.* 1999), as well as through grazing (Archer *et al.* 2001, Simó *et al.* 2018) and viral attack (Bratbak *et al.* 1995, Hill *et al.* 1998, Malin *et al.* 1998). Once released, DMSP is partially transformed into dimethylsulphide (DMS) through the action of enzymatic lyase activity (Stefels *et al.* 2007). As a volatile, part of the DMS escapes into the atmosphere, where it evolves by oxidation into secondary aerosols that eventually contribute to cloud condensation nuclei and cloud brightness, thereby impacting climate (Vogt & Liss 2009).

There is still only limited knowledge regarding the physicochemical properties and microbial composition of the SML in Antarctic sea waters, particularly regarding the abundance, diversity and ecological roles of DMSP-producing phototrophic phytoplankton (e.g. *Phaeocystis antarctica*) and their associated viruses (e.g. haptophyte viruses or giant viruses). With the aim to fill this knowledge gap, we sampled viral and microbial communities in the SML and SSW across three different areas along the western Antarctic Peninsula during two cruises: PEGASO (2015) and PI-ICE (2019). We assessed the abundances of viruses, prokaryotes and heterotrophic and phototrophic nanoflagellates, paying particular attention to the abundance of phototrophic nanoflagellates with high DMSP contents (e.g. *Phaeocystis*-like species) and their potential viruses. These results were compared with measurements of seawater temperature, salinity, dissolved organic carbon (DOC), DMSP and inorganic nutrient concentrations, as well as atmospheric UV radiation and wind speed, which all have the potential to affect the microbial communities in the SML.

Materials and methods

Sampling regions and strategy

The PEGASO and PI-ICE cruises were conducted on board the research vessel (R/V) *BIO-Hespérides* and at the Spanish Antarctic Base (BAE). PEGASO was carried out between 8 January and 13 February 2015, whereas PI-ICE took place between late January and mid-March 2019. The latter included sampling in both open ocean waters (21 January 2019–5 February 2019) and coastal waters (6 February 2019–13 March 2019) near Livingston Island, where BAE is located. Altogether, a total of 20 samplings were carried out in three different regions (Bellingshausen Sea, Gerlache Passage and the Bransfield Strait coastal area; Fig. 1 & Table I). The SML was sampled under calm sea conditions from a rubber boat at ≥ 1 nautical mile from the research vessel or from the shore to avoid contamination. The SML samples were obtained using a glass plate sampler (Fig. S1; Stortini *et al.* 2012), which had been previously cleaned with acid over 12 h and rinsed thoroughly with ultrapure water (Milli-Q water). To ascertain the extent of any procedural contamination, field SML blanks were collected by rinsing and collecting 0.5 l of ultrapure water. A glass plate of 975 cm^2 surface area was used, and ~100 dips were required to collect 500 ml of the SML water. The SSW samples were collected just underneath the microlayer at between 0.1 and 0.5 m either manually with a clean jar (PI-ICE cruise) or with a 10 cm tube attached to a floating device and siphoned with a syringe (PEGASO cruise). Both SML and SSW samples were stored in acid-cleaned plastic carboys until they were processed either onboard the vessel or at the BAE laboratory. For chemical and microbiological measurements, between 600 ml and 1 l were collected from the SML, and 2 l were collected from the SSW. To determine whether higher values for all variables were observed in the SML compared to the SSW, we calculated the enrichment factor (EF) for both chemical and biological parameters. The EF is defined as the ratio of the concentration or abundance in the SML to that in the SSW. An EF of > 1.0 indicated an enrichment in the SML relative to the SSW, whereas an EF of < 1.0 indicated a depletion in the SML relative to the SSW.

Environmental variables

Temperature was only measured in the SSW immediately after sampling on the rubber boat using a calibrated thermometer. Samples for salinity were collected for both layers when feasible and stored refrigerated in a cool box for later analysis in the R/V *BIO-Hespérides* laboratory using a Portasal Guildline 8410-A salinometer, which determines practical salinity based on conductivity ratios according to the Practical Salinity Scale 1978 (PSS-78). Therefore, as practical salinity is a dimensionless quantity under the PSS-78 scale, no units are required (UNESCO 1981). Duplicate 10 ml samples for the determination of the dissolved inorganic nutrients nitrate (NO_3^-), nitrite (NO_2^-), ammonia (NH_4^+), silicate (SiO^{4-}_4) and phosphate (PO_4^{3-}) were kept frozen at -20°C (Becker *et al.* 2020) until analysis on a Bran-Luebbe AA3 HR autoanalyser (3 months after sampling back to the laboratory of the Institute of Marine Sciences (ICM-CSIC)) according to standard spectrophotometric methods (Hansen & Koroleff 1999). Samples for DOC analyses were filtered through a glass fibre filter (GF/F), and 30 ml aliquots were transferred to duplicate glass ampoules pre-combusted at 450°C for 5 h, sealed under flame and stored until analysis in the ICM-CSIC laboratory. The DOC analyses were conducted using a Shimadzu total organic carbon TOC-5000 or TOC-Vcsh instrument, employing high-temperature catalytic oxidation techniques as described by Spyres *et al.* (2000). Standards provided by D.A. Hansell and W. Chen (University of Miami) of 2 and 44 μmol l^{-1} DOC were employed to assess the accuracy of the estimates. For the analysis of DMSP, two pellets of sodium hydroxide (NaOH) were added to 30 ml of unfiltered seawater samples in glass vials for 24 h hydrolysis to DMS. Aliquots of between 0.1 and 1.0 ml were injected into a purge flask containing high-purity water, purged for a period of 4–6 min with ultrapure helium and analysed for evolved DMS using a gas chromatography system with a flame photometric detector. The concentration of DMSP was calculated by subtracting the endogenous DMS. PEGASO samples were analysed onboard, whereas PI-ICE samples were stored after

https://doi.org/10.1017/S0954102025100205 Published online by Cambridge University Press

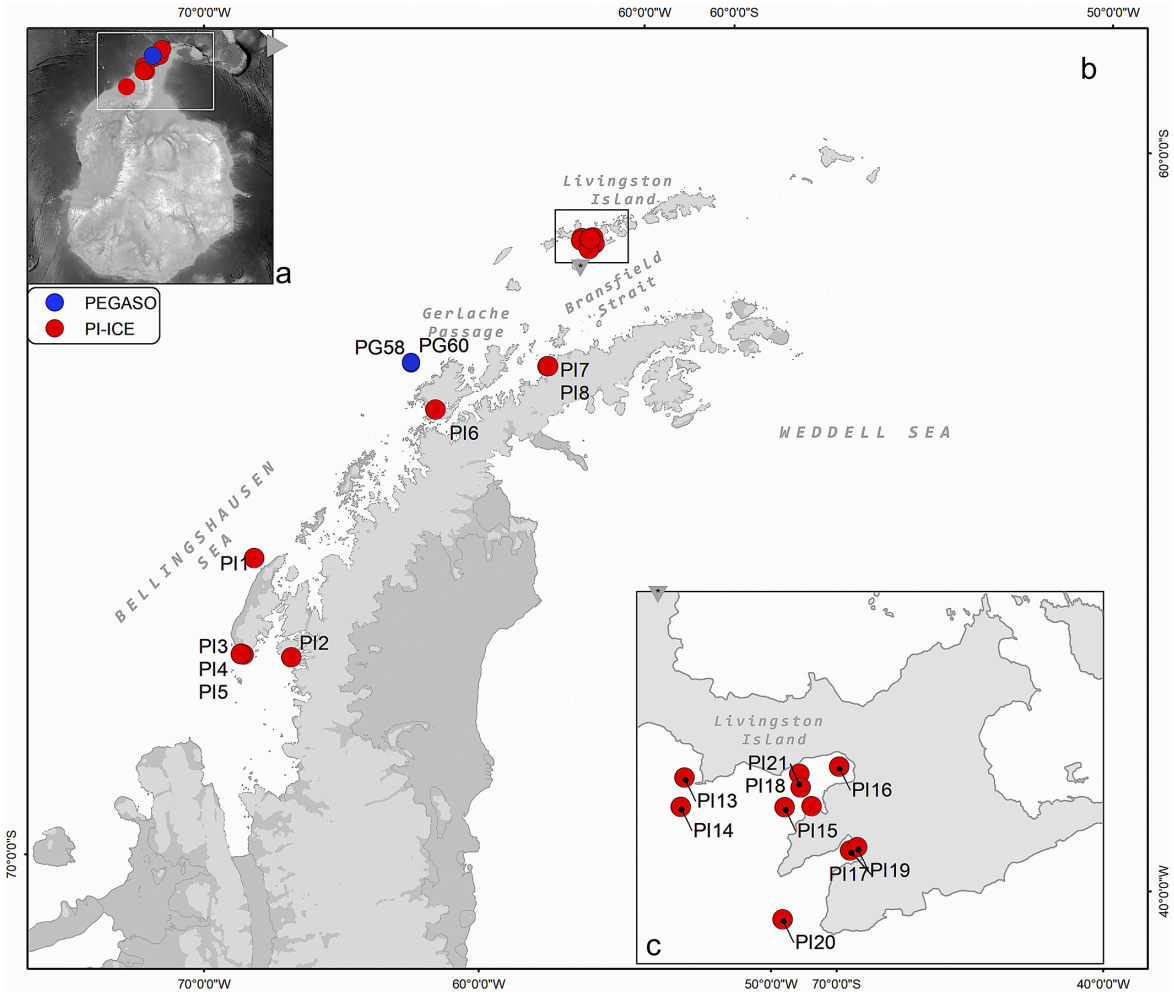

Figure 1. a. Map with the location of the study area. **b.** Sampling sites along the western Antarctic Peninsula: Bellingshausen Sea, Gerlache Passage and Bransfield Strait. **c.** Zoomed-in window of the stations of the Bransfield Strait coastal area.

the addition of NaOH and analysed at the ICM-CSIC laboratory in Barcelona within 4 months of the cruise. The measurements of wind speed and UV radiation were obtained from a Aanderaa Scanning Unit 3010 Automatic Weather Station, which was situated in the upper part of the *BIO-Hespérides*, and the automatic meteorological station (EMA) WMO 89064, sited in Livingston Island, not far from the BAE. Wind speed was transformed to a standard height of 10 m by means of a power law with an exponent of 0.11 (Hsu *et al.* 1994). The values of UV radiation (290–390 nm) were obtained at 10 min intervals using a UV Davis 6490 sensor. The UV data were displayed in terms of irradiance and a UV index. The UV index is based on erythemal exposure, which is defined as the level of UV radiation that causes reddening of the skin. The UV index was calculated by dividing the erythemal-weighted global irradiance by 25 mW m^{-2} (Kerr & Fioletov 2007).

Viral and microbial abundances

Subsamples (2 ml) were collected from the SML and the SSW for the enumeration of viruses and prokaryotes (heterotrophic bacteria and archaea) through flow cytometry (Brussaard 2004, Gasol & Del Giorgio 2000, respectively). The samples were previously fixed with glutaraldehyde (0.5% final concentration) for viruses and with P+G (paraformaldehyde (P) 1% + glutaraldehyde (G) 0.05%) for prokaryotes. Both were maintained at 4°C for 15–30 min in the dark and then flash-frozen in liquid nitrogen and stored at −80°C until analysis. The enumeration was conducted using a FACSCalibur flow cytometer at the ICM-CSIC laboratory up to 2 months after sampling. Samples for viral abundance (VA) were diluted with TE buffer (10:1 mM Tris:EDTA), stained with SYBR Green I and analysed at a medium flow speed (Brussaard 2004), with a flow rate of 58–64 µl min^{-1}. The presence of viruses was determined through the use of bivariate scatter plots, which employed the green fluorescence of stained nucleic acids in conjunction with the side scatter (Brussaard 2004). Depending on their green fluorescence and side scatter signals, we identified four distinct virus populations (V1–V4). Presumably, the V1 and V2 populations are dominated by bacteriophages (Biggs *et al.* 2021). The V3 and V4 fractions typically comprise eukaryotic viruses (Fig. S2; Evans *et al.* 2009). In particular, the V4 fraction has been found to correspond to viruses infecting members of the Haptophyceae, such as *Phaeocystis* species (Brussaard *et al.* 1999, 2005). Samples for prokaryotic abundance (PA) were stained with SYTO13 (SYTO™ 13, ThermoFisher) and enumerated by flow cytometry in accordance with the methodology outlined by Gasol & Del Giorgio (2000). Prokaryotic cells were identified based on their distinctive signatures in a plot of 90° light scatter (SSC) *vs* green fluorescence (FL1; Fig. S2; Gasol *et al.* 1999). Subsamples (30 ml) for the

https://doi.org/10.1017/S0954102025100205 Published online by Cambridge University Press

Table I. Date, location, zone, Station (St) and environmental conditions of the sampled stations during the PEGASO (PG) and PI-ICE (PI) cruises. Temperature (Temp) and salinity were collected at 10 cm depth. Irradiation and wind speed were measured from the corresponding sensors located in the research vessel *BIO-Hespérides* and in the Spanish Antarctic Base (BAE) (see 'Materials and methods' section).

Data	Latitude	Longitude	Zone	St	Temp (°C)	Salinity	Irradiation (W m^{-2})	UV index	Wind Speed(m s^{-1})
25 January 2019	−66.6607	−68.5541	Bel S	PI1	−0.8	30.9	88.6	4	6.2
26 January 2019	−67.7946	−67.3316	"	PI2	1.8	29.9	267.9	11	4.2
27 January 2019	−67.7818	−68.8026	"	PI3	1.0	32.4	300.8	12	3.5
27 January 2019	−67.7701	−68.8739	"	PI4	0.8	32.4	300.8	12	3.5
27 January 2019	−67.7758	−68.8789	"	PI5	0.7	32.5	300.8	12	3.5
29 January 2019	−64.8146	−63.7725	GP	PI6	NA	31.8	117.8	5	5.5
30 January 2019	−64.1525	−60.9679	"	PI7	1.0	33.0	107.3	4	4.3
30 January 2019	−64.1538	−60.9513	"	PI8	0.0	33.2	107.3	4	4.3
2 February 2015	−64.3214	−64.5316	"	PG58	1.4	33.4	163.3	7	4.6
3 February 2015	−64.3022	−64.5361	"	PG60	1.4	33.4	458.7	18	13.3
21 February 2019	−62.6578	−60.3927	Br S	PI12	2.2	-	151.9	6	1.2
22 February 2019	−62.6515	−60.6375	"	PI13	3.0	33.4	221.6	9	2.7
22 February 2019	−62.6772	−60.6356	"	PI14	3.0	33.1	221.6	9	2.7
25 February 2019	−62.6628	−60.4422	"	PI15	2.3	32.9	112.2	4	1.7
1 March 2019	−62.6201	−60.3543	"	PI16	0.0	29.8	199.4	8	2.5
2 March 2019	−62.6903	−60.3074	"	PI17	−0.1	30.7	64.7	3	1.5
6 March 2019	−62.6322	−60.4253	"	PI18	2.1	32.1	85.4	3	3.5
9 March 2019	−62.6860	−60.2949	"	PI19	0.5	30.1	50.2	2	1.7
9 March 2019	−62.7583	−60.4109	"	PI20	0.5	30.9	50.2	2	1.7
11 March 2019	−62.6434	−60.4188	"	PI21	4.3	31.5	55.4	2	1.9

Bel S = Bellingshausen Sea; Br S = Bransfield Strait; GP = Gerlache Passage.

enumeration of nanoflagellates were fixed with glutaraldehyde (1% final concentration), filtered through 0.6 µm black polycarbonate filters and stained with 4,6-diamidino-2-phenylindole (DAPI) at a final concentration of 5 µg ml^{-1} (Sieracki *et al.* 1985). Counts of heterotrophic nanoflagellates (HNFs) and phototrophic nanoflagellates (PNFs) were conducted using epifluorescence microscopy (Olympus BX40-102/E at 1000×), with a blue wavelength excitation filter (bandpass (BP) 460–490 nm) and barrier (emission) filter (BA; 510–550 nm), and with an UV excitation filter (BP 360–370 nm) and barrier filter (BA 420–460 nm). PNFs and HNFs were distinguished under blue light, where the presence of plastidic structures in the PNFs could be observed as red fluorescence. A minimum of 20–100 cells of each type of nanoflagellate were counted per sample and separated into size classes of ≤ 2, 2–5, 5–10 and 10–20 µm. *Phaeocystis*-like species (Fig. S3) were predominantly observed in the 2–5 µm PNF size class.

Data analyses

The Shapiro-Wilk *W*-test was used to test the normality of the data, and the Levene's test was used to test for homogeneity of variance from means. Data were logarithmically transformed prior to analysis, if necessary. Pearson correlation and linear regression analyses were applied to evaluate the relationships between the different biotic and environmental parameters. One-way analyses of variance (ANOVAs) were conducted to investigate the differences in physicochemical and biological variables between the SML and the SSW for the entire region and individual zones, as well as the differences in SML and SSW values among the various zones. These analyses were conducted using *Kaleidagraph* 5.01 (copyright 1986–2021 by Synergy Software) and the *PAST4* app 1.06. Multivariate statistical analyses were conducted using *R* version 4.3.2 (R Core Team 2023). For principal component analysis (PCA), *tidyverse* version 1.3 (Wickham & RStudio 2023) and *dplyr* (Wickham *et al.* 2023a) were employed for data handling and manipulation. The *prcomp* function from the *stats* package, version 3.6.2 (Bolar 2019), was employed to conduct the PCA, which yielded the principal components and explained variances. To facilitate the interpretation of the results of the PCA, the packages *factoextra* version 1.0.7 (Kassambara & Mundt 2020) and *ggplot2* version 3.4.4 (Wickham *et al.* 2023b) were used together to create detailed and customized plots. The PCA included variables with enough coincident data in order not to introduce noise into the analyses. Thus, nutrient concentrations and some microbial abundances and VAs were not included.

Results

Environmental and physicochemical parameters

During both cruises, UV radiation varied between 2 and 18 UV index, with the lowest value recorded in the Bransfield Strait and the highest in the Gerlache Passage (Table I). A similar pattern was

https://doi.org/10.1017/S0954102025100205 Published online by Cambridge University Press

observed for wind speed, with minimum (1.2 m s^{-1}) and maximum (13.3 m s^{-1}) values recorded in the same areas as for the UV index (Table I). The two variables were positively correlated (r = 0.599, P < 0.01, Tables S1 & S2). The temperature and salinity values recorded in the SSW ranged from the coldest (−0.8°C) in the Bellingshausen Sea to the warmest (4.3°C) in the Bransfield Strait. Salinity was also lowest (29.9) in the Bellingshausen Sea and highest (33.4) in the Gerlache Passage and Bransfield Strait, with both these areas being close to the coast (Table I).

Almost all inorganic and organic compounds, except silicate (SiO_4^{4-}), showed a significant positive correlation between the SML and SSW layers (Table S3). Regarding the inorganic nutrients, there were no significant differences between the layers, except for SiO_4^{4-} (Table S4). When comparing the SML of the three sampled areas, SiO_4^{4-} showed significantly higher values in the Gerlache Passage than in the Bransfield Strait. For NO_3^-, NO_2^- and NH_4^+, their concentrations exhibited the opposite trend to that of SiO_4^{4-}, being higher in the Bransfield Strait than in the Gerlache Passage (Tables II & S4). In the case of SSW, all inorganic nutrients showed lower values in the Bellingshausen Sea than in the other two areas (Tables II & S4). A similar pattern of high values for NO_2^-, NO_3^- and PO_4^{3-} in the Bransfield Strait for both layers is reflected in the strong positive correlations among them in both the SML and SSW (Tables S1 & S2). Furthermore, the occurrence of a high DOC concentration was observed exclusively within the Bransfield Strait (Table II). Finally, DMSP concentrations were higher in the SML than in the SSW only in some sites of the Gerlache Passage and Bransfield Strait. Over the entire cruise, DMSP was on average 113.7 ± 21.3 nM (range of 24.5–206.7 nM) in the SML and 111.6 ± 23.1 nM (range of 22.6–268.9 nM) in the SSW. The highest and the lowest concentrations were observed in the Bransfield Strait, and the cruise average for the EF was ~1 (Table II).

Viral and microbial variables

Viral and microbial abundances in both layers were significantly and positively correlated, meaning that they followed a similar pattern (Table S3) and did not show significant differences between the SML and the SSW (Table S4). However, in most cases, the averaged EF was ≥ 1, indicating a tendency to have higher values in the SML than in the SSW (Table III). PAs in the SML ranged from 1.6×10^5 to 9.7×10^5 cells ml^{-1}, with a mean of $5.0 \times 10^5 \pm 5.7 \times 10^4$ cells ml^{-1}, whereas in the SSW they averaged $4.3 \times 10^5 \pm 5.2 \times 10^4$ (range of 1.2×10^5–9.0×10^5 cells ml^{-1}), with the highest mean EF of 1.70 ± 0.41 recorded in the Bransfield Strait (Fig. 2a & Table III). Significantly higher abundances were observed in the SML of the Bellingshausen Sea and Bransfield Strait than in the SML of the Gerlache Passage (Table S4).

The mean total VA was higher in the SML (mean of $3.5 \times 10^6 \pm 5.5 \times 10^5$ viruses ml^{-1}) than in the SSW (mean of $3.0 \times 10^6 \pm 4.8 \times 10^5$ viruses ml^{-1}), but this difference was not significant (Table III). A total of 14 cases out of 19 showed higher VAs in the SML than in the SSW (Fig. 2b). Furthermore, the mean EFs in the three regions were similar (Table III). The lowest abundances were observed in the Bransfield Strait for both the SML and the SSW (0.7×10^6 and 0.8×10^6 viruses ml^{-1}, respectively), whereas the highest abundances for both the SML and SSW were recorded in the Gerlache Passage (1.4×10^7 and 1.3×10^7 viruses ml^{-1}, respectively; Fig. 2b & Table III). Similarly, three of the virus populations (V1 and V2 mainly being bacteriophages and V3 mainly infecting pico- and nanoeukaryotes) exhibited the highest abundance values in the Gerlache Passage and the lowest abundance values in the Bransfield Strait (Table III), whereas the opposite was observed for the V4 population abundance, with the lowest abundance in the Gerlache Passage (Table III). Additionally, V4 was the only group that displayed average EF values ≤ 1, especially in the Bellingshausen Sea and Gerlache Passage. These different spatial dynamics of the V4 population were reflected in the significant correlation between VAs with V1, V2 and V3 but not with V4 (Tables S1 & S2). In particular, the V4 population was identified as a potential specific virus of *Phaeocystis*-like species, which were abundantly present in the SML and SSW samples, mainly in the Bransfield Strait, coinciding with the highest abundance of PNFs within the 2–5 µm size class (Table III).

The mean abundance of HNFs in the SML was $1.2 \times 10^3 \pm 0.2 \times 10^3$ cells ml^{-1} (range of 0.4×10^3–3.2×10^3 cells ml^{-1}), and in the SSW this value was $1.5 \times 10^3 \pm 0.2 \times 10^3$ (range of 0.6×10^3–2.8×10^3 cells m^{-1}; Fig. 2c & Table III). The EF values displayed considerable variability (Table III): in 9 out of 17 cases, the abundance of HNFs exhibited higher values in the SSW than in the SML, and average EF values only exceeded 1 in the Bransfield Strait (Table III). The HNF 2–5 µm size fraction is considered to primarily contain bacterivores, representing a substantial proportion of the total HNF abundance (up to 76%, ranging from 14% to 75% in the SML and from 25% to 76% in the SSW). This is also reflected in the significant correlation between the abundance of HNFs and the HNF 2–5 µm size fraction in both layers, as well as in the SML (r = 0.888, P < 0.005) and in the SSW (r = 0.947, P < 0.005; Tables S1 & S2). In the SML, this size class exhibited both the lowest (0.08×10^3 cells ml^{-1}) and the highest abundances in the Bransfield Strait (2.4×10^3 cells ml^{-1}). In the SSW, the abundance ranged from 0.15×10^3 cells ml^{-1} in the Bellingshausen Sea to 1.5×10^3 cells ml^{-1} in the Bransfield Strait. The abundance of the HNF 10–20 µm size fraction was relatively low (Table III), yet it was the sole size class that exhibited significant interlayer differences in the Bellingshausen Sea (Table S4). Furthermore, the abundance of this fraction was significantly higher in the SML of this region than in the SML of the Gerlache Passage and Bransfield Strait (Table S4). However, the HNF ≤ 2 µm size fraction abundance was higher in the SSW of the Bransfield Strait than in the SSW of the Gerlache Passage and Bellingshausen Sea (Table S4).

Potential virus-PNF interaction and its relationship with DMSP concentration

The abundance of PNFs, similarly to the other microbial variables, did not present significant differences between the SML and SSW layers (Table S4). The mean abundance of PNFs in the SML was $3.8 \times 10^3 \pm 1.4 \times 10^3$ cells ml^{-1}, which is slightly higher than that observed in the SSW ($3.6 \times 10^3 \pm 1.3 \times 10^3$ cells ml^{-1}; Fig. 3a), and the average value of EFt (pooling the three areas) was 1.20 ± 0.13 (Table III). In both SML and SSW layers, the lowest and the highest values were observed in the Bransfield Strait (0.5×10^3–22.7×10^3 cells ml^{-1} and 0.5×10^3–21.5×10^3 cells ml^{-1}, respectively). Regarding the existence of significant differences in both layers between the sampled areas, only the abundance of the PNF ≤ 2 µm size fraction in the SML showed lower values in the Bellingshausen Sea than in the Bransfield Strait and Gerlache Passage (Tables III & S4). The PNF 2–5 µm size fraction includes *Phaeocystis*-like species, which belong to small haptophytes known for their high intracellular DMSP content. These organisms represent a substantial portion of the total PNF abundance in both the SML and SSW. In the SML, they accounted for an average of

https://doi.org/10.1017/S0954102025100205 Published online by Cambridge University Press

https://doi.org/10.1017/S0954102025100205 Published online by Cambridge University Press

Table II. Averages, minimum and maximum values and enrichment factors (EFs) of physicochemical variables registered in the Bellingshausen Sea, Gerlache Passage and Bransfield Strait at the surface microlayer (SML) and subsurface water (SSW) layers, and the EF average (EFt) for all pooled areas. Concentrations of nitrate (NO_3^-), nitrite (NO_2^-), ammonia (NH_4^+), silicate (SiO_4^{4-}), phosphate (PO_4^{3-}), dissolved organic carbon (DOC) and dimethylsulphoniopropionate (DMSP) are shown. EF and EFt averages in bold correspond to values ≥ 1.0.

Variables	Bellingshausen Sea			Bellingshausen Sea Gerlache Passage			Bransfield Strait			EFt Average ± SE
	SML	SSW	EF	SML	SSW	EF	SML	SSW	EF	
	Average (minimum - maximum)	Average (minimum - maximum)	Average ± SE	Average (minimum - maximum)	Average (minimum - maximum)	Average ± SE	Average (minimum - maximum)	Average (minimum - maximum)	Average ± SE	
Temperature (°C)	-	**0.7** (–0.8–1.8)	-	-	**0.8** (0.0–1.4)	-	.	**1.7** (–0.1–4.3)	-	-
Salinity	**31.6** (30.4–32.3)	**31.6** (29.9–32.5)	**1.01** ± 0.0	**32.1** (31.2–33.3)	**33.0** (31.8–33.4)	0.98 ± 0.01	**31.7** (29.6–33.3)	**31.9** (30.1–33.4)	0.99 ± 0.01	0.99 ± 0.02
NO_3^- (μM)	-	**15.5** (1.5–23.2)	-	**20.3** (16.6–24.1)	**19.8** (14.5–24.3)	**1.01** ± 0.07	**23.9** (21.2–27.3)	**24.8** (19.9–28.8)	0.95 ± 0.03	0.97 ± 0.03
NO_2^- (μM)	-	**0.15** (0.07–0.19)	-	**0.17** (0.10–0.25)	**0.20 (**0.12–0.26)	0.95 ± 0.08	**0.24** (0.22–0.30)	**0.25** (0.20–0.29)	0.99 ± 0.04	0.99 ± 0.04
NH_4^+ (μM)	-	**0.66** (0.23–1.52)	-	**1.13** (0.04–2.01)	**0.89** (0.04–1.97)	**1.14** ± 0.13	**1.53** (0.04–3.71)	**1.90** (0.04–8.76)	**2.58** ± 1.33	**2.19** ± 1.10
SiO_4^{4-} (μM)	-	**49.9** (42.7–62.1)	-	**62.9** (53.9–77.7)	**74.3** (54.0–87.8)	0.87 ± 0.11	**49.7** (45.3–53.6)	**79.0** (41.6–108.6**)**	0.69 ± 0.08	0.74 ± 0.07
PO_4^{3-} (μM)	-	**0.83** (0.17–1.44)	-	**1.46** (1.24–1.75)	**1.59 (**1.28–1.77)	0.96 ± 0.02	**1.67** (1.33–1.86)	**1.63** (1.37–1.90)	**1.02** ± 0.02	**1.01** ± 0.02
DOC (μM)	-	**76.5** (59.0–147.6)	-	**62.0** (59.6–64.4)	**54.4** (47.9–63.8)	**1.03** ± 0.09	**227.0** (105.2–456.2)	**216.1** (50.5–670.6)	**1.54** ± 0.24	**1.45** ± 0.21
DMSP (nM)	**85.8** (45.9–112.6)	**83.4** (54.4–106.5)	0.97 ± 0.05	**82.9** (32.6–137.5)	**78.0** (83.2–112.0)	**1.07** ± 0.29	**142.8** (24.5–206.7)	**155.4** (22.6–268.9)	**1.07** ± 0.03	**1.04** ± 0.07

SE = standard error.

Table III. Averages, minimum and maximum values and enrichment factors (EFs) registered in the three sampled areas at the surface microlayer (SML) and subsurface water (SSW) layers of the Bellingshausen Sea, Gerlache Passage and Bransfield Strait and the EF average (EFt) for all pooled areas. Abundances of prokaryotes (PA), total viruses (VA), viral populations (V1–V4), heterotrophic nanoflagellates (HNFs), size fractions of HNFs (2–20 μm), phototrophic nanoflagellates (PNFs) and size fractions of PNFs (2–20 μm) are shown. EF and EFt averages in bold corresponded to values ≥ 1.0.

Variables	Bellingshausen Sea			Gerlache Passage			Bransfield Strait			EFt Average ± SE
	SML	SSW	EF	SML	SSW	EF	SML	SSW	EF	
	Average (minimum - maximum)	Average (minimum - maximum)	Average ± SE	Average (minimum - maximum)	Average (minimum - maximum)	Average ± SE	Average (minimum - maximum)	Average (minimum - maximum)	Average ± SE	
PA (10^5 ml^{-1})	**5.8** (1.6–8.2)	**5.9** (1.2–9.0)	**1.0** ± 0.07	**2.7** (1.7–4.9)	**2.6** (1.6–4.9)	**1.1** ± 0.05	**5.7** (3.1–9.7)	**4.4** (3.0–6.7)	**1.7** ± 0.41	**1.4** ± 0.21
VA (10^6 ml^{-1})	**3.1** (1.9–4.2)	**2.6** (1.6–3.6)	**1.1** ± 0.04	**6.2** (1.9–13.6)	**5.4** (1.4–12.8)	**1.1** ± 0.05	**2.7** (0.7–4.1)	**2.8** (0.8–6.2)	**1.3** ± 0.16	**1.1** ± 0.08
V1	**1.4** (0.8–2.1)	**1.1** (0.6–1.4)	**1.2** ± 0.06	**2.7** (0.9–7.0)	**2.0** (0.8–4.3)	**1.3** ± 0.13	**1.4** (0.3–2.0)	**1.4** (0.3–3.8)	**1.2** ± 0.15	**1.2** ± 0.08
V2	**1.5** (0.9–2.2)	**1.3** (0.8–1.8)	**1.2** ± 0.05	**2.2** (0.7–4.3)	**2.2** (0.6–4.4)	**1.1** ± 0.06	**0.8** (0.2–1.3)	**0.8** (0.2–1.8)	**1.2** ± 0.15	**1.1** ± 0.09
V3	**0.06** (0.02–0.1)	**0.04** (0.02–0.04)	**2.3** ± 0.59	**0.2** (0.04–0.6)	**0.2** (0.04–0.6)	**1.0** ± 0.16	**0.03** (0.005–0.06)	**0.04** (0.006–0.07)	**1.4** ± 0.30	**1.5** ± 0.23
V4	**0.2** (0.1–0.3)	**0.3** (0.2–0.4)	0.6 ± 0.06	**0.09** (0.02–0.1)	**0.09** (0.03–0.2)	0.9 ± 0.12	**0.5** (0.2–1.3)	**0.5** (0.2–1.2)	**1.1** ± 0.16	0.9 ± 0.11
HNF (10^2 ml^{-1})	**6.6** (4.4–8.8)	**10.1** (6.2–17.8)	0.9 ± 0.19	**10.2** (8.0–13.2)	**14.9** (7.5–21.3)	0.8 ± 0.23	**17.8** (5.3–32.4)	**15.8**(9.7–27.7)	**1.2** ± 0.25	**1.0** ± 0.16
HNF ≤ 2 μm	**0.2** (0.1–0.3)	**1.8** (0.9–3.5)	0.2 ± 0.16	**1.3** (0.3–2.3)	**1.7** (0.9–2.4)	0.7 ± 0.27	**5.4** (0.1–21.5)	**5.3** (1.3–12.8)	**1.2** ± 044	0.9 ± 0.31
HNF 2–5 μm	**2.5** (2.2–2.9)	**5.6** (1.5–11.9)	**1.0** ± 0.32	**4.5** (2.7–6.4)	**7.7** (3.0–11.2)	0.8 ± 0.35	**9.2** (0.8–24.1)	**5.6** (4.3–14.9)	**1.2** ± 0.30	**1.1** ± 0.19
HNF 5–10 μm	**2.3** (2.1–2.5)	**1.9** (1.3–3.6)	**1.3** ± 0.21	**4.0** (1.9–5.1)	**5.2** (2.5–7.7)	0.8 ± 0.07	**3.1** (0.4–7.1)	**2.7** (0.3–6.7)	**1.4** ± 0.33	**1.3** ± 0.28
HNF 10–20 μm	**2.2**(1.4–3.6)	**0.7** (0.3–1.4)	**3.3** ± 1.42	**0.4** (0.1–0.6)	**0.6** (NA–0.6)	0.2 ± 0.00	**0.3** (0.1–0.6)	**0.4** (0.1–0.9)	**1.7** ± 1.4	**2.1** ± 0.65
PNF (10^2 ml^{-1})	**14.9** (6.7–29.2)	**10.5** (6.3–12.7)	**1.4** ± 0.37	**26.0** (18.5–31.7)	**28.1** (18.5–35.8)	**0.9** ± 0.08	**51.0** (5.1–227.3)	**48.8** (5.3–215.3)	**1.1** ± 0.15	**1.2** ± 0.13
PNF ≤ 2 μm	**0.8** (0.1–2.4)	**2.0** (0.1–3.5)	**1.1** ± 0.77	**3.9** (2.2–5.8)	**4.8** (3.9–6.1)	0.9 ± 0.31	**1.5** (0.9–2.3)	**1.7** (0.3–3.8)	**1.5** ± 0.75	**1.3** ± 0.45
PNF 2–5 μm	**6.3** (4.6–9.7)	**5.3** (3.2–9,3)	**1.6** ± 0.49	**15.5** (8.9–24.4)	**18.9** (11.9–22.6)	0.9 ± 0.23	**48.3** (4.1–217.5)	**47.4** (3.9–201.9)	**1.2** ± 0.21	**1.2** ± 0.21
PNF 5–10 μm	**2.1** (0.5–4.4)	**1.4** (0.4–2.9)	**2.6** ± 2.21	**2.6** (0.9–5.3)	**0.8** (0.3–1.5)	**5.0** ± 2.32	**0.8** (0.1–7.6)	**1.4** (0.1–8.6)	**1.2** ± 0.30	**2.5** ± 0.83
PNF 10–20 μm	**6.2** (0.3–12.7)	**1.8** (0.06–4.5)	**2.8** ± 0.49	**4.1** (0.3–7.7)	**3.6** (0.3–9.0)	**1.6** ± 0.63	**0.2** (0.2–1.7)	**0.6** (0.3–1.0)	0.7 ± 0.22	**1.1** ± 0.24

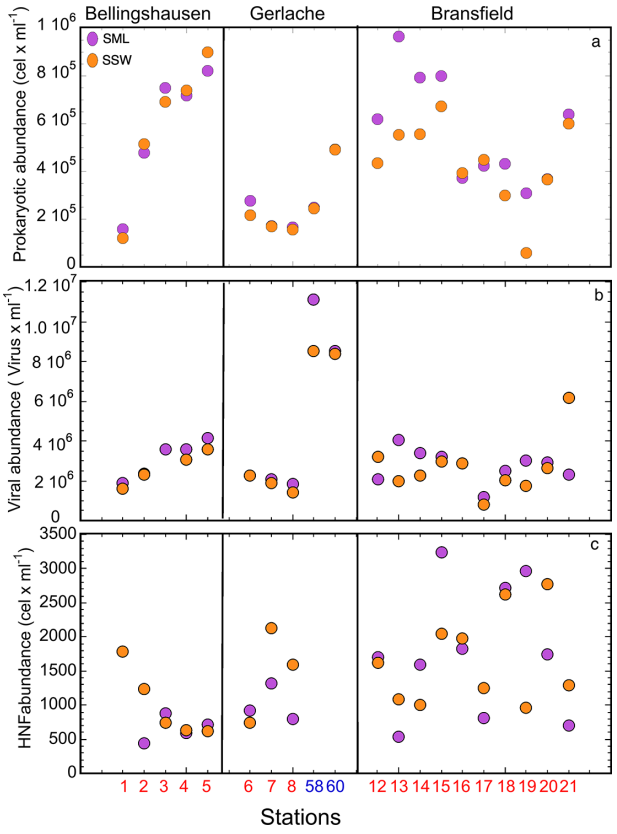

Figure 2. Abundances of **a.** prokaryotes, **b.** viruses and **c.** heterotrophic nanoflagellates (HNFs) for the sampling stations in the three areas at the surface microlayer (SML) and subsurface waters (SSW) of the sampling stations. Station numbers in blue are from PEGASO and those in red are from PI-ICE cruises.

74% ± 5.4%, with values ranging from 32% in the Bellingshausen Sea to 99.4% in the Bransfield Strait. Similar proportions were observed in the SSW, where they represented an average of 74% ± 5%, ranging from 27% to 99% in the same regions. Cell concentrations of these protists averaged $3.3 \times 10^3 \pm 1.3 \times 10^3$ cells ml^{-1} in the SML (ranging from 0.4×10^3 to 21.7×10^3 cells ml^{-1}) and $3.0 \times 10^3 \pm 1.3 \times 10^3$ cells ml^{-1} in the SSW (ranging from 0.3×10^3 to 20.2×10^3 cells ml^{-1}; Fig. 3a,b). Furthermore, the concentration of DMSP showed a similar distribution in both layers and in the three areas (Fig. 3c). However, the abundance of the viral (V4) population (supposed to include PNF viruses) followed the concentration of PNFs and the PNF 2–5 µm size fraction only in the SML (Fig. 3a,b,d). As expected, we observed that the DMSP concentration and the abundances of PNFs and the PNF 2–5 µm size fraction (e.g. *Phaeocystis*-like species) were significantly and positively related, both in the SML and in the SSW, with similar slopes (Fig. 4a,b). In contrast, the V4 population abundance was only significantly related to PNFs and the PNF 2–5 µm size fraction in the SML, explaining 45% and 57% of the variance, respectively, and not in the SSW (Fig. 4c,d).

Relationships among all microbial variables in the three areas

To gain an overview of the relationships among all coincident viral (VA), microbial (PA, HNF, PNF, including the size classes) and environmental variables (UV, wind speed, salinity and temperature) analysed across all areas and layers, we performed a multivariate analysis (PCA; Fig. 5a). We selected PC1 and PC2 for visualization because they explain the largest proportions of variance in the dataset (34.3% and 28.1%, respectively). Although PC3 explained 10.5% of the variance, it did not contribute to additional biological or ecological separation, so we excluded it for clarity. Overall, the samples did not show any clustering concerning sampling zones (Bellingshausen Sea, Gerlache Passage and Bransfield Strait) or water layers (SML and SSW). When we examined the contribution of the most relevant variables to the first principal component (PC1; Fig. 5b), we found that the total abundance of PNFs, the different size classes (PNF 2–5 µm and PNF 5–10 µm), the concentration of DMSP and the abundance of V4 were the most significant contributors (> 13%). In addition, Fig. 5a shows that all of these variables have high-quality scores (cos2 > 0.8) and point in the same direction along the PC1 axis. This reflects that these four variables are well correlated (Tables S1 & S2). As can be seen in Fig. 4d and Table S1, the correlation is especially high between V4 and the PNF 2–5 µm size fraction in the SML. On the other hand, UV radiation, total VA, V2 and V3 and PA appear to explain most of the variance along the PC2 axis (Fig. 5c).

Discussion

In the present study, we aimed to test the hypothesis that the DMSP concentration in the SML would be largely determined by the abundance of *Phaeocystis*-like species cells, and that the interaction of these cells with their specific viruses (V4) would be stronger in the SML than in the SSW. Despite the weak enrichment of microorganisms in the sampled SMLs, we observed a potential interaction of V4 and *Phaeocystis*-like species mainly in this layer, which is consistent with the release of DMSP as a major precursor of DMS, an important aerosol compound that contributes to cloud formation.

Overall, most microbial variables were slightly enriched in the SML (EF > 1; Table III). This enrichment could be due to the upwards transport of microorganisms attached to buoyant particles or bubble scavenging, as reported in other studies (Joux *et al.* 2006, Vaqué et al. 2021). The averaged EF values for PA (1.0–1.6) and total VA (1.1–1.2) were comparable to those previously reported by Joux *et al.* (2006) and Zäncker *et al.* (2021) in the Mediterranean, and they were also slightly lower than those observed by Vaqué *et al.* (2021) in polar systems. Even at some stations in the Bellingshausen Sea (PI2, PI4 and PI5) and in the Bransfield Strait (PI16 and PI17), the EF was less than 1 for PA, whereas for VA it was less than 1 only in the Bransfield Strait (PI12 and PI21). These lower abundances in the SML than in the SSW are in agreement with previous reports, where similar low EFs were detected in some locations of the polar systems (Vaqué et al. 2021), the Mediterranean Sea (Joux *et al.* 2006) and Halong Bay (Pradeep Ram *et al.* 2018). In addition, EFs < 1 have been recorded for PA in the subtropical Atlantic Gyre, in the western Mediterranean (Reinthaler *et al.* 2008) and in Raunafjorden, Norway (Cunliffe *et al.* 2009). Furthermore, the SML was weakly enriched in HNFs and PNFs (mean EFt = 1.0 ± 0.2 and 1.2 ± 0.1, respectively) and diminished (mean EF < 1) mainly in the Gerlache Passage (Table III). Depletion of nanoflagellates in the SML has already been observed in the Arctic Ocean (Vaqué et al. 2021). In contrast, Joux *et al.* (2006) and Zäncker *et al.* (2021) both found nanoflagellate enrichment in the Mediterranean Sea. However, Zäncker *et al.* (2021) observed larger differences in the diversity of picoeukaryotic communities between the sampling sites than between SML and SSW. In our study, even though we

https://doi.org/10.1017/S0954102025100205 Published online by Cambridge University Press

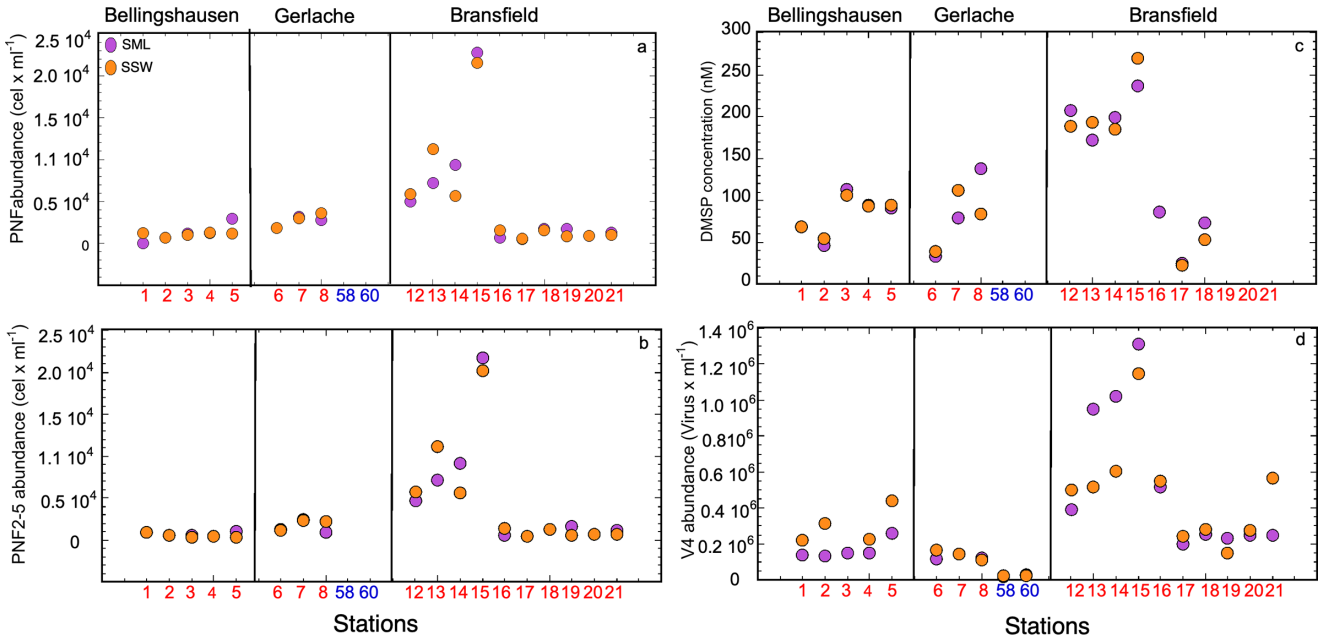

Figure 3. Abundances of **a.** total phototrophic nanoflagellates (PNFs) and **b.** phototrophic nanoflagellates (2–5 μm; PNF2–5), **c.** dimethylsulphoniopropionate (DMSP) concentration and **d.** V4 population abundance at the surface microlayer (SML) and subsurface waters (SSW) of the sampling stations. Station numbers in blue are from PEGASO and those in red are from PI-ICE cruises.

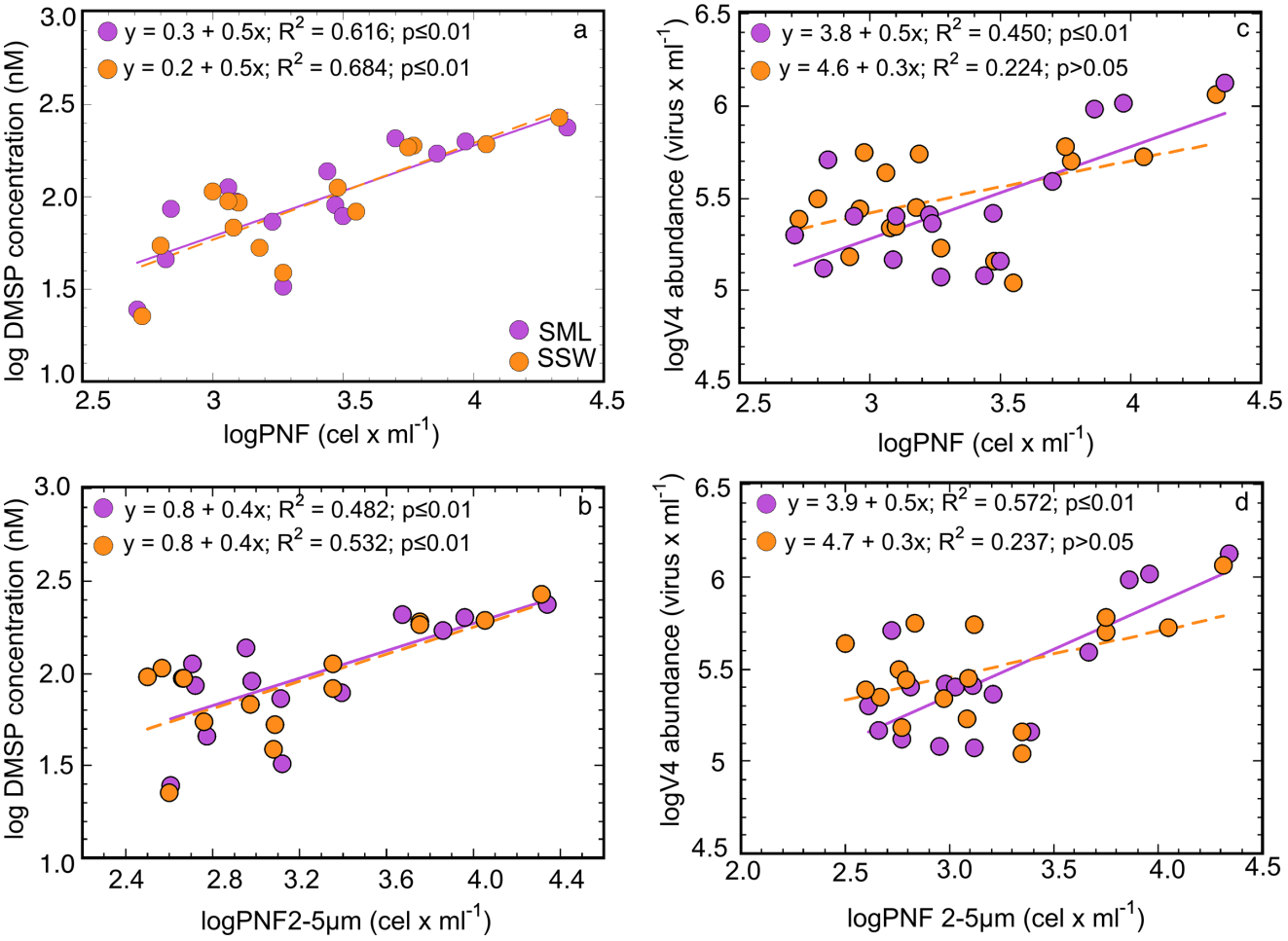

Figure 4. Linear regression analyses between dimethylsulphoniopropionate (DMSP) concentration and **a.** phototrophic nanoflagellates (PNFs) and **b.** the PNF 2–5 μm size fraction abundances, as well as between V4 abundance and **c.** PNF and **d.** the PNF 2–5 μm size fraction abundances in the sampling stations and from the surface microlayer (SML) and the subsurface waters (SSW).

https://doi.org/10.1017/S0954102025100205 Published online by Cambridge University Press

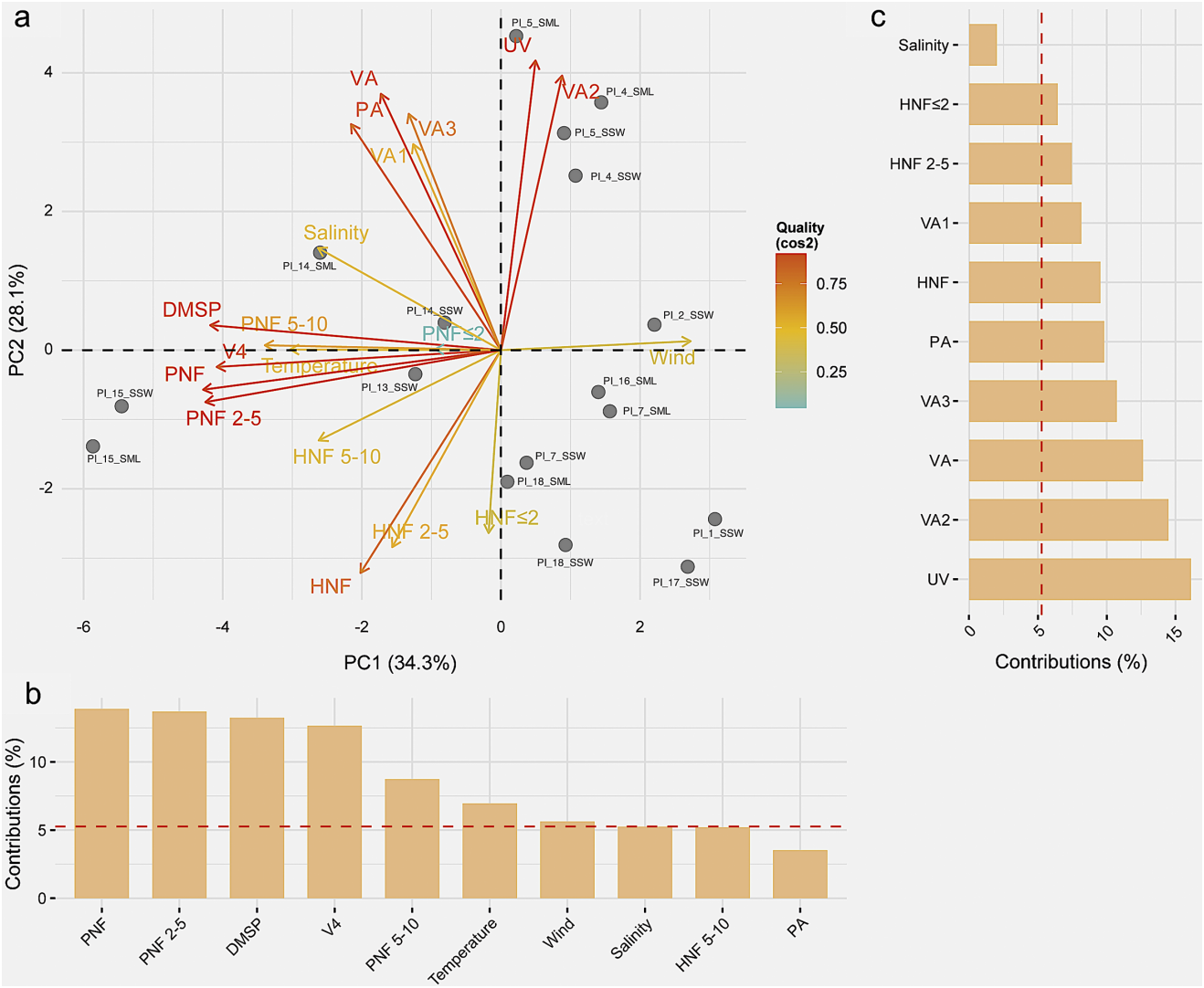

Figure 5. a. Principal component analysis biplot of the distribution of the samples and variables in the first two principal components (PCs). The colour of each arrows indicates the quality of the representation (cos2) of the variable on the PCs. The size of each arrows represents the contribution of the variable to the PCs. The axes represent the percentage of variance explained by each component: the first component (PC1) explains 34.3% of the variance, whereas the second component (PC2) explains 28.1%. **b.** Contribution of the variables to PC1. **c.** Contribution of the variables to the PC2. The dashed red lines represent the average contribution thresholds. DMSP = dimethylsulphoniopropionate; HNF = heterotrophic nanoflagellate; PA = prokaryotic abundance; PNF = phototrophic nanoflagellate; UV = ultraviolet; VA = viral abundance.

do not have taxonomic indicators of diversity, we can take the size classes as an approximate indicator of the composition of the nanoflagellate assemblages. In the SML, the abundances of the PNF ≤ 2 µm size fraction were significantly lower in the Bellingshausen Sea compared to in the Gerlache Passage and Bransfield Strait, whereas the PNF 10–20 µm size fraction exhibited significantly higher abundances in the Bellingshausen Sea. No differences in the abundances of PNF size classes were observed between the SSW of the different sampled areas (Table S4). Unlike microbial variables, no enrichment in the EF was observed for physicochemical variables, except for ammonium and DOC in the Bransfield Strait (Table II).

The lack of clear differences between the layers could be due to the mixing of the SML and the SSW caused by the wind (Wurl *et al.* 2011). Even though we did not observe strong winds during the study (range of 1.2–13.3 m s^{-1}), except for during 1 day in the Gerlache Passage (Table I), there was a slight decrease in EF for microbial abundances, VA, V4, PNFs and DMSP concentration at wind speeds > 4 m s^{-1} (Table IV). These results are consistent with reports for marine waters elsewhere (Engel *et al.* 2017, Rahlff *et al.* 2017). In the SML, wind speed was significantly negatively correlated with V4 abundance and marginally negatively correlated with DMSP concentration (Table S1). Furthermore, in the PCAs, wind speed showed an opposite influence on these variables and on total PNFs and for the different PNF size classes (Fig. 5). In contrast, although high levels of UV radiation could potentially cause cell damage or photoinhibition or be involved in the decrease of the EF for viruses and microorganisms in the SML (Buma *et al.* 2001, Bigg *et al.* 2004), in our study we did not detect any significant statistical relationship of UV with PNFs, even when high radiation was observed (Fig. 5 & Table IV). Zäncker *et al.* (2021) showed that phytoplankton abundance was greater in the SML despite high radiation levels, and Vaqué et al. (2021) observed that VA and viral activity were not affected by UV. However, HNF abundances showed low EF values (Table III) and were negatively correlated with UV (Table S1), suggesting that this radiation can

https://doi.org/10.1017/S0954102025100205 Published online by Cambridge University Press

Table IV. Enrichment factors (EFs) of abundances of prokaryotes (PA), viruses (VA), V4 viral population (V4), phototrophic nanoflagellates (PNFs), *Phaeocystis*-like species (PNF 2–5 μm) and dimethylsulphoniopropionate (DMSP) concentration under different wind speed and ultraviolet (UV) index conditions. Figures within parentheses indicate ranges for wind speed and UV index irradiation.

	n	EF (PA)	*n*	EF (VA)	*n*	EF (V4)	*n*	EF (PNF)	*n*	EF (PNF 2–5 μm)	*n*	EF (DMSP)
Wind speed												
≤ 4 m s^{-1}	13	1.5 ± 0.3	12	1.2 ± 0.1	12	1.0 ± 0.1	13	1.2 ± 0.2	13	1.3 ± 0.2	9	1.1 ± 0.05
≥ 4 m s^{-1}	7	1.1 ± 0.06	7	1.1 ± 0.05	7	0.8 ± 0.1	4	0.9 ± 0.08	4	0.9 ± 0.2	4	1.0 ± 0.3
(1.2–13.5 m s^{-1})												
UV index												
≤ 5	10	1.5 ± 0.4	10	1.1 ± 0.1	10	0.9 ± 0.1	9	1.1 ± 0.1	9	1.2 ± 0.2	6	1.1 ± 0.2
≥ 5	10	1.1 ± 0.04	9	1.2 ± 0.1	9	1.0 ± 0.2	8	1.2 ± 0.3	8	1.2 ± 0.3	7	1.0 ± 0.04
(2–18)												

be detrimental to HNFs. This is consistent with the study of Ochs (1996), in which increasing doses of UV radiation were shown to cause a decrease in the HNF abundance and in grazing rates.

The measured DMSP concentrations (23–269 nM) were within the range of previous observations in productive polar regions in summer, representing the waters and season with the highest DMSP concentrations in the global surface ocean (Galí *et al.* 2015). DMSP enrichment in the SML only occurred in 5 out of 14 sampling sites (Fig. 3c); overall, DMSP had an EF that was not significantly different from 1. Another recent study in the northern Southern Ocean also did not find enrichment in the SML (Saint-Macary *et al.* 2023). However, several previous studies had reported such enrichments (Yang & Tsunogai, 2005, Zemmelink *et al.* 2006), particularly in productive waters where dinoflagellates were dominant among the phytoplankton (Yang 1999, Matrai *et al.* 2008, Yang *et al.* 2009). Dinoflagellates were not the most abundant group in our studied waters, with their highest concentration being recorded in the SSW of the Bellingshausen Sea at 87 cells ml^{-1} (M. Delgado, personal observation 2021). Instead, the waters were dominated by PNFs, as shown in Table III.

Despite the weak or no enrichment of all parameters in the SML, the abundances of PNFs (total PNFs and *Phaeocystis*-like species) and DMSP concentration were significantly correlated, showing similar slopes in both SML and SSW (Fig. 4a). Indeed, many phytoplankton taxa included in the PNF abundances as haptophytes (e.g. *Phaeocystis*-like species) are recognized as major DMSP producers (Keller 1989, Stefels *et al.* 2007). Subsequently, we found that the putative specific viruses (V4) of *Phaeocystis*-like species, with an average EF of 1.2 ± 0.2, showed a highly significant positive relationship with these PNFs exclusively in the SML (Fig. 4c,d & Table III). This result suggests that *Phaeocystis*-like species and their viruses were more strongly associated in this layer than in the SSW. The lysed cells would then release DMSP into the upper layer, promoting DMS production through microbial activity (Brussaard *et al.* 2006).

Conclusions

Our results expand our understanding of the spatial variability of physicochemical, viral and microbial parameters in the SML and SSW across three regions of the Antarctic Peninsula. Almost all variables showed significant correlations between the SML and SSW, indicating a strong exchange between the two layers. Overall, there was low enrichment in the SML for each of the assessed parameters across the different areas, which may be partly explained by wind speed disrupting the stability of the microlayer and promoting mixing with the underlying water. Nevertheless, a significant relationship was observed between the abundances of PNFs and *Phaeocystis*-like species with DMSP concentration, both in the SML and in the SSW. Additionally, a significant correlation was found exclusively in the SML between *Phaeocystis*-like species and the abundances of their putative specific viruses (V4). Although the abundances of V4, *Phaeocystis*-like species, PNFs and DMSP are not markedly higher in the SML than in the SSW, their stronger correlations in the SML than in the SSW could reflect a more cohesive environment, where biogeochemical and ecological processes are more tightly interconnected. This suggests that the release of DMSP from those photosynthetic microorganisms may occur predominantly in this upper layer, where it is subsequently transformed into volatile DMS and emitted into the atmosphere through the air-sea interface.

Supplementary material. To view supplementary material for this article, please visit http://doi.org/10.1017/S0954102025100205.

Acknowledgements. We thank our colleagues S. Zeppenfeld, M. van Pinxteren, D.C.S. Beddows, J. Brean and C. Garcia-Botín for their invaluable assistance with sampling and laboratory work, and particularly to Dr M. Delgado, for the phytoplankton observations using the inverted microscope. DOC analyses were carried out by M. Abad (ICM-CSIC). We also thank the crew of the R/V *BIO-Hespérides* for enabling the field study, for their hospitality and for their logistical support. We are especially indebted to the Unidad de Tecnología Marina, and in particular to M. Ojeda and J. Riba, for their technical and logistical support at the Spanish Antarctic Base (BAE). We thank the TREC expedition (Tara Oceans) for their visit to the ICM, during which they provided confocal images of our Antarctic samples. This study was conducted as part of the POLARCSIC platform activities and was also supported by the institutional framework of the 'Severo Ochoa Centre of Excellence' accreditation (CEX2019-000928-S).

Financial support. The study was supported by the Spanish Ministry of Economy through projects PEGASO (CTM2012-37615) to R. Simó, BIO-NUC (CGL2013-49020-R) to M. Dall'Osto and PI-ICE (CTM2017-89117-R) to E. Berdalet and M. Dall'Osto.

Competing interests. The authors declare none.

Authors contribution. Conceptualization: DV, MMS. Fieldwork, sample and data analyses: EB, ME, AS-G, MC-B, MM-N, AR, XL-A, MV, CM. Writing - original draft: DV, EB, MMS. Revisions of the final draft: ME, RS, MD'O. Funding acquisition: EB, RS, MD'O. All authors approved the final version of the manuscript.

Dedication. This study is dedicated to the memory of our colleague and friend Dr Andrés Barbosa.

References

Archer, S.D., Stelfox-Widdicombe, C.E., Burkill, P.H. & Malin, G. A. 2001. Dilution approach to quantify the production of dissolved dimethylsulphoniopropionate and dimethyl sulphide due to microzooplankton herbivory. *Aquatic Microbial Ecology*, **23**, 131–154.

Becker, S., Aoyama, M., Woodward, E.M.S., Bakker, K., Coverly, S., Mahaffey, C. & Tanhua, T. 2020. GO-SHIP repeat hydrography nutrient manual: the precise and accurate determination of dissolved inorganic nutrients in seawater, using continuous flow analysis methods. *Frontiers in Marine Sciences*, **7**, 10.3389/fmars.2020.581790.

Bigg, E.K., Leck, C. & Tranvik, L. 2004. Particulates of the surface microlayer of open water in the central Arctic Ocean in summer. *Marine Chemistry*, **91**, 131–141.

Biggs, T.E.G, Huisman, J. & Brussaard, C.P.D. 2021. Viral lysis modifies seasonal phytoplankton dynamics and carbon flow in the Southern Ocean. *ISME Journal*, **15**, 10.1038/s41396-021-01033-6.

Bolar, K. 2019. *STAT*: interactive document for working with basic statistical analysis (version 0.1.0) [software]. Retrieved from https://cran.r-project.org/web/packages/STAT/index.html

Bratbak, G., Levasseur, M., Michaud, S., Cantin, G., Fernandez, E., Heimdal, B.R. & Heldal, M. 1995 Viral activity in relation to *Emiliania huxleyi* blooms: a mechanism of DMSP release? *Marine Ecology Progress Series*, **128**, 133–142.

Brussaard, C.P.D. 2004. Optimization of procedures for counting viruses by flow cytometry. *Applied Environmental and Microbiology*, **70**, 10.1128/AEM.70.3.1506-1513.2004.

Brussaard, C.P.D., Kuipers, B. & Veldhuis, M.J.W. 2005. A mesocosm study of *Phaeocystis globosa* population dynamics: I. Regulatory role of viruses in bloom control. *Harmful Algae*, **4**, 10.1016/j.hal.2004.12.012.

Brussaard, C.P.D., Bratbak, G., Baudoux, A.C. & Ruardij, P. 2006. *Phaeocystis* and its interaction with viruses. *Biogeochemistry*, **83**, 10.1007/s10533-007-9096-0.

Brussaard, C.P.D., Thyrhaug, R., Marie, D. & Bratbak, G. 1999. Flow cytometric analyses of viral infection in two marine phytoplankton species, *Micromonas pusilla* (Prasinophyceae) and *Phaeocystis pouchetii* (Prymnesiophyceae). *Journal of Phycology*, **35**, 10.1046/j.1529-8817.1999.3550941.x.

Buma, A.G.J., Helbing, E.W., de Boer, M.K. & Villafañe, V.E. 2001. Patterns of DNA damage and photoinhibition in temperate South-Atlantic picophytoplankton exposed to solar ultraviolet radiation. *Journal of Photochemistry and Photobiology*, **62**, 9–18.

Cunliffe, M., Salter, M., Mann, P.J., Whiteley, A., Upstill-Goddard, R.C. & Murrell, J.C. 2009. Dissolved organic carbon and bacterial populations in the gelatinous surface microlayer of a Norwegian fjord mesocosm. *FEMS Microbiology Letters*, **299**, 248–254.

Cunliffe, M., Engel, A., Frka, S., Gasparovic, B., Guitart, C., Murrell, J.C., *et al.* 2013. Sea surface microlayers: a unified physicochemical and biological perspective of the air-ocean interface. *Progress in Oceanography*, **1109**, 104–116.

Dall'Osto, M., Ovadnevaite, J., Paglione, M., Beddows, D.C.S., Ceburnis, D., Cree, C., *et al.* 2017. Antarctic sea ice region as a source of biogenic organic nitrogen in aerosols. *Scientific Reports*, **7**, 10.1038/s41598-017-06188-x.

Engel, A., Bange, H.W., Cunliffe, M., Burrows, S.M., Friedrichs, G., Galgani, L., *et al.* 2017. The ocean's vital skin: toward an integrated understanding of the sea surface microlayer. *Frontiers in Marine Sciences*, **4**, 10.3389/fmars.2017.00165.

Evans, C., Pearce, I. & Brussard, C.P.D. 2009. Viral-mediated lysis of microbes and carbon release in the sub-Antarctic and Polar Frontal zones of the Australian Southern Ocean. *Environmental Microbiology*, **11**, 2924–2934.

Galí, M., Devred, E., Levasseur, M., Royer, S.-J. & Babin, M. 2015. A remote sensing algorithm for planktonic dimethylsulfoniopropionate (DMSP) and an analysis of global patterns. *Remote Sensing of Environment*, **171**, 171–184.

Gasol, J.M. & del Giorgio, P.A. 2000. Using flow cytometry for counting natural planktonic bacteria and understanding the structure of planktonic bacterial communities. *Scientia Marina*, **64**, 10.3989/scimar.2000.64n2197.

Gasol, J.M., Zweifel, U.L., Peters, F., Fuhrman, J.A. & Hagström, Å. 1999. Significance of size and nucleic acid content heterogeneity as measured by flow cytometry in natural planktonic bacteria. *Applied Environmental and Microbiology*, **65**, 10.1128/AEM.65.10.4475-4483.1999.

Gowing, M.M., Garrison, D.L., Gibson, A.H., Krupp, J.M., Jeffires, M.O. & Fritsen, C.H. 2004. Bacterial and viral abundance in Ross Sea summer pack ice communities. *Marine Ecology Progress Series*, **279**, 3–12.

Hansen, H.P. & Koroleff, F. 1999. Determination of nutrients. *In* Grasshoff, K., Kremling, K. & Ehrhardt, M., *eds*, *Methods of seawater analysis*, 3rd edition. Hoboken, NJ: Wiley, 10.1002/9783527613984.ch10.

Hardy, J.T. 1982. The sea-surface microlayer: biology, chemistry and anthropogenic enrichment. *Progress in Oceanography*, **11**, 307–328.

Hill, R.W., White, B.A., Cottrell, M.T. & Dacey, J.W. 1998. Virus-mediated total release of dimethylsulfoniopropionate from marine phytoplankton: a potential climate process. *Aquatic Microbial Ecology*, **14**, 1–6.

Hsu, S.A., Meindl, E.A. & Gilhousen, D.B. 1994. Determining the power-law wind-profile exponent under near-neutral stability conditions at sea. *Journal of Applied Meteorology*, **33**, 757–765.

Joux, F., Agogué, H., Obernosterer, I., Dupuy, C., Reinthaler, T., Herndl, G.J. & Lebaron, P. 2006. Microbial community structure in the sea surface microlayer at two contrasting coastal sites in the northwestern Mediterranean Sea. *Aquatic Microbial Ecology*, **42**, 91–104.

Kassambara, A. & Mundut, F. 2020. Extract and visualize the results of multivariate data analyses (version 1.0.7) [software]. Retrieved from https://project.org/web/packages/factoextra/index.html

Keller, M.D. 1989 Dimethyl sulfide production and marine phytoplankton: the importance of species composition and cell size. *Biology and Oceanography*, **6**, 375–382.

Kerr, J.E. & Fioletov, V.E. 2007. Surface ultraviolet radiation. *Atmosphere-Ocean*, **46**, 10.3137/ao.460108.

Kuznetsova, M. & lee, C. 2001. Enhanced extracellular enzymatic peptide hydrolysis in the sea-surface microlayer. *Marine Chemistry*, **73**, 319–332.

Laroche, D., Vezina, A.F., Levasseur, M., Gosselin, M., Stefels, J., Keller, M.D., *et al.* 1999. DMSP synthesis and exudation in phytoplankton: a modeling approach. *Marine Ecology Progress Series*, **180**, 37–49.

Liss, P.S. & Duce, R.A. 1997. *The sea surface and global change*, 1st edition . Cambridge: Cambridge University Press, 537 pp.

Malin, G., Wilson, W.H., Bratbak, G., Liss, P.S. & Mann, N.H. 1998. Elevated production of dimethylsulfide resulting from viral infection of cultures of *Phaeocystis pouchetii*. *Limnology and Oceanography*, **43**, 1389–1393.

Martinez-Varela, A., Casas, G., Piña, B., Dachs, J. & Vila-Costa, M. 2020. Large enrichment of anthropogenic organic matter degrading bacteria in the sea-surface microlayer at coastal Livingston Island (Antarctica). *Frontiers in Microbiology*, **11**, 571983.

Matrai, P.A. & Keller, M.D. 1994. Total organic sulfur and dimethylsulfoniopropionate in marine phytoplankton: intracellular variations. *Marine Biology*, **119**, 61–68.

Matrai, P.A., Tranvik, L., Leck, C. & Knulst, J.C. 2008. Are high Arctic surface microlayers a potential source of aerosol organic precursors? *Marine Chemistry*, **108**, 10.1016/j.marchem.2007.11.001.

Nakajima, R., Tsuchiya, K., Nakatomi, N., Yoshida, T., Tada, Y., Konno, F., *et al.* 2013. Enrichment of microbial abundance in the sea-surface microlayer over a coral reef: implications for biogeochemical cycles in reef ecosystems. *Marine Ecology Progress Series*, **490**, 10.3354/meps10481.

Obernosterer, I., Catala, P., Lami, R., Caparros, J., Ras, J., Bricaud, A., *et al.* 2008. Biochemical characteristics and bacterial community structure of the sea surface microlayer in the south Pacific Ocean. *Biogeosciences*, **5**, 10.5194/bg-5-693-2008.

Ochs, C.A. 1996. Effects of UV radiation on grazing by two marine heterotrophic nanoflagellates on autotrophic picoplankton. *Journal of Plankton Research*, **10**, 1517–1536.

Pradeep Ram, A.S., Mari, X., Brune, J., Torreton, J.P., Chu, V.T., Raimbault, P., *et al.* 2018. Bacterial-viral interactions in the sea surface microlayer of a black carbon-dominated tropical coastal ecosystem (Halong Bay, Vietnam). *Elementa Science of the Anthropocene*, **6**, 10.1525/elementa.276.

Rahlff, J. 2019. The virioneuston: a review on viral-bacterial associations at air-water interfaces. *Viruses*, **11**, 191.

Rahlff, J., Stolle, C., Giebel, H.A., Brinkhoff, T., Ribas-Ribas, M., Hodapp, D. & Wurl, O. 2017. High wind speeds prevent formation of a distinct bacterioneuston community in the sea-surface microlayer. *FEMS Microbiology Ecology*, **93**, 10.1093/femsec/fix041.

Reinthaler, T., Sintes, E. and Herndl, G.J. 2008. Dissolved organic matter and bacterial production and respiration in the sea-surface microlayer of the open Atlantic and the western Mediterranean Sea. *Limnology and Oceanography*, **53**, 122–136.

Saint-Macary, A.D., Marriner, A., Barthelmeß, T., Deppeler, S., Safi, K., Costa Santana, R., *et al.* 2023. Dimethyl sulfide cycling in the sea surface microlayer in the southwestern Pacific - part 1: enrichment potential determined using a novel sampler. *Ocean Science*, **19**, 10.5194/os-19-1-2023.

Sellegri, K., Nicosia, A., Freney, E., Uitz, J., Thyssen, M., Grégori, G., *et al.* 2021. Surface ocean microbiota determine cloud precursors. *Scientific Reports*, **11**, 10.1038/s41598-020-78097-5.

Sieracki, M.E., Johnson, P.W. & Sieburth, J.M. 1985. Detection, enumeration, and sizing of planktonic bacteria by image-analyzed epifluorescence microscopy. *Applied Environmental and Microbiology*, **49**, 799–810.

Simó, R. 2001. Production of atmospheric sulfur by oceanic plankton: biogeochemical, ecological and evolutionary links. *Trends in Ecology and Evolution*, **16**, 287–294.

Simó, R., Saló, V., Almeda, R., Movilla, J., Trepat, I., Saiz, E. & Calbet, A. 2018. The quantitative role of microzooplankton grazing in dimethylsulfide (DMS) production in the NW Mediterranean. *Biogeochemistry*, **141**, 125–142.

Sotomayor-Garcia, A., Sala, M.M., Ferrera, I., Estrada, M., Vázquez-Domínguez, E., Emelianov, M., *et al.* 2020. Assessing viral abundance and community composition in four contrasting regions of the Southern Ocean. *Life*, **10**, 10.3390/life10070107.

Spyres, G.S.G., Worsfold, P.J., Miller, E.P.A., Mimmo, M. & Miller, A.J. 2000. Determination of dissolved organic carbon in seawater using high-temperature catalytic oxidation techniques. *Trends in Analytical Chemistry*, **19**, 498–506.

Stefels, J., Steinke, M., Turners, S., Malin, G. & Belviso, S. 2007. Environmental constraints on the production and removal of the climatically active gas dimethylsulphide (DMS) and implications for ecosystem modelling. *Biogeochemistry*, **83**, 245–275.

Steiner, P.A., Sintes, E., Simó, R., de Corte, D., Pfannkuchen, D.M., Ivancic I., *et al.* 2019. Seasonal dynamics of marine snow-associated and free-living demethylating bacterial communities in the coastal northern Adriatic Sea. *Environmental Microbiology Reports*, **11**, 10.1111/1758-2229.12783.

Stortini, A.M., Cincinelli, A., Degli Innocenti, N., Tovar-Sánchez, A. & Knulst, J. 2012. Surface microlayer. *In* Pawliszyn, J., *ed.*, *Comprehensive sampling and sample preparation*. Oxford: Oxford Academic Press, 223–246.

Tovar- Sánchez, A., González-Ortegón, E. & Duarte, C.M. 2019. Trace metal partitioning in the top meter of the ocean. *Science of the Total Environment*, **652**, 907–914.

Tréguer, P. & Jacques, G. 1992. Dynamics of nutrients and phytoplankton, and fluxes of carbon, nitrogen and silicon in the Antarctic Ocean. *Polar Biology*, **12**, 10.1007/BF00238255.

UNESCO. 1981. *Background papers and supporting data on the Practical Salinity Scale 1978*. UNESCO Technical Papers in Marine Science, **37**. Paris: UNESCO, 140 pp.

Vaqué, D., Boras, J.A., Arrieta, J.M., Agustí, S., Duarte, C.M. & Sala, M.M. 2021. Enhanced viral activity in the surface microlayer of the Arctic and Antarctic oceans. *Microorganisms*, **9**, 10.3390/microorganisms9020317.

Vogt, M. & Liss, P.S. 2009. Dimethylsulfide and climate. *In* Le Quére, Ć. & Saltzman, E.S., *eds*, *Surface ocean - lower atmosphere processes*. Washington, DC: AGU Press, 197–232.

Wickham, H. RStudio. 2023. *tidyverse:* easily install and load the 'tidyverse' (version 2.0.0) [software]. Retrieved from https://cran.r-project.org/web/packages/tidyverse/index.html

Wickham, H., François, R., Henry, L., Müller, K. & Vaughan, D. 2023a. *dplyr*: a grammar of data manipulation. Retrieved from https://CRAN.R-project.org/package=dplyr

Wickham, H., Chang, W., Henry, L., Pedersen, T.L., Takahashi, K., Wilke, C., *et al.* 2023b. *ggplot2*: create elegant data visualisations using the grammar of graphics (version 3.4.4) [software]. Retrieved from https://cran.r-project.org/web/packages/ggplot2/index.html

Wurl, O., Wurl, E., Miller, L., Johnson, K. & Vagle, S. 2011. Formation and global distribution of sea-surface microlayers. *Biogeosciences*, **8**, 121–135.

Yang, G.-P. 1999. Dimethylsulfide enrichment in the surface microlayer of the South China Sea. *Marine Chemistry*, **66**, 10.1016/S0304-4203(99)00042-0.

Yang, G.-P. & Tsunogai, S. 2005. Biogeochemistry of dimethylsulfide (DMS) and dimethylsulfoniopropionate (DMSP) in the surface microlayer of the western North Pacific. *Deep-Sea Research I*, **52**, 10.1016/j.dsr.2004.11.013.

Yang, G.-P., Levasseur, M., Michaud, S., Merzouk, A., Lizotte, M. & Scarratt, M. 2009. Distribution of dimethylsulfide and dimethylsulfoniopropionate and its relation with phytoneuston in the surface microlayer of the western North Atlantic during summer. *Biogeochemistry*, **94**, 10.1007/s10533-009-9323-y.

Zäncker, B., Cunliffe, M. & Engel A. 2021. Eukaryotic community composition in the sea surface microlayer across an east-west transect in the Mediterranean Sea. *Biogeosciences*, **18**, 10.5194/bg-18-2107-2021.

Zemmelink, H.J., Houghton, L., Frew, N.M. & Dacey, J.W.H. 2006. Dimethylsulfide and major sulfur compounds in a stratified coastal salt pond. *Limnology and Oceanography*, **51**, 10.4319/lo.2006.51.1.0271.

https://doi.org/10.1017/S0954102025100205 Published online by Cambridge University Press